A Generalized Voltage Droop Strategy for Control of Multiterminal DC Grids

Kumars Rouzbehi, *Student Member, IEEE*, Arash Miranian, *Student Member, IEEE*,
Jose Ignacio Candela, *Member, IEEE*, Alvaro Luna, *Member, IEEE*, and Pedro Rodriguez, *Fellow, IEEE*

***Abstract*—This paper proposes a generalized voltage droop (GVD) control strategy for dc voltage control and power sharing in voltage source converter (VSC)-based multiterminal dc (MTDC) grids. The proposed GVD control is implemented at the primary level of a two-layer hierarchical control structure of the MTDC grid, and constitutes an alternative to the conventional voltage droop characteristics of voltage-regulating VSC stations, providing higher flexibility and, thus, controllability to these networks. As a difference with other methods, the proposed GVD control strategy can be operated in three different control modes, including conventional voltage droop control, fixed active power control, and fixed dc voltage control, by adjusting the GVD characteristics of the voltage-regulating converters. Such adjustment is carried out in the secondary layer of the hierarchical control structure. The proposed strategy improves the control and power-sharing capabilities of the conventional voltage droop, and enhances its maneuverability. The simulation results, obtained by employing a CIGRE B4 dc grid test system, demonstrate the efficiency of the proposed approach and its flexibility in active power sharing and power control as well as voltage control. In these analysis, it will be also shown how the transitions between the operating modes of the GVD control does not give rise to active power oscillations in the MTDC grids.**

***Index Terms*—CIGRE B4 dc grid test system, generalized voltage droop (GVD) control, multiterminal dc (MTDC) grids, power sharing.**

I. Introduction

THE research conducted in the field of voltage source converter (VSC)-based multiterminal dc (MTDC) grids, including modeling and simulation [1]–[3], short-circuit calculation [4], protection [5], [6], and control [7]–[9], has experienced an outstanding evolution over the last years. Such popularity is mainly due to two reasons: appropriateness of the MTDC grids for the integration of offshore wind farms and possibility of interconnecting several (more than two) ac networks with even nonidentical frequencies.

The high-voltage MTDC grids are advantageous compared to conventional ac transmission for the integration of offshore distant wind generation into the ac mainland, due to their capability for transmitting high power over long distances [10]. At the present time, there are several ongoing projects worldwide for transmission of bulk offshore wind generations to the ac networks via the MTDC grids [11]–[13]. Moreover, efforts are being made for developing the "European Supergrid" with MTDC grids as its backbone [11]. Likewise, there are also proposals for a subsea MTDC grid around the North Sea to collect the rich wind resource of the region and also interconnect the U.K. and Nordic pool with continental Europe [14].

DC voltage control, active power control, and power sharing are essential operational tasks in MTDC grids in order to guarantee the proper performance of the grid. This is due to the fact that, in a dc network, the flow of energy between the network's terminals is governed by the terminal's dc voltage. Unlike ac systems where synchronization parameter (i.e., frequency) is maintained at the nominal value throughout the system, the dc voltage in the MTDC grids cannot be set to a same level for all terminals. In fact, there must be a strategy for controlling the dc voltage in the MTDC grids, in such a way that the desirable power flow is realized between the dc terminals.

Three main strategies can be identified for dc voltage control in MTDC grids, i.e., master–slave strategy, voltage margin strategy, and voltage droop strategy. While in the master–slave approach always one VSC is responsible for controlling the voltage profile and others control the flow of power [15], the voltage-regulation task can be shifted among several VSCs in the voltage margin strategy [15]. Obviously, the master–slave method suffers from poor reliability since the dc voltage control is totally lost if the master converter fails. However, the voltage margin method, which can be seen as an extension of master–slave control, experiences some drawbacks, too. For instance, oscillations are generated in the dc voltages when the master converter is shifted [16].

In the voltage droop control, as the most commonly employed strategy for dc voltage control in the MTDC grids, several converters contribute to the dc voltage control of the grid [17]. In this approach, which originated from power–frequency droop control in ac systems, the voltage-regulating converters will share the power based on the slope of their voltage droop characteristics. The voltage droop control exhibits a higher reliability compared to the master–slave control, and does not

K. Rouzbehi, J. I. Candela, and A. Luna are with the Department of Electrical Engineering, Technical University of Catalonia, 08222 Terrassa, Spain (e-mail: kumars.rouzbehi@upc.edu; candela@ee.upc.edu; luna@ee.upc.edu).

A. Miranian is with the Young Researchers and Elite Club, Mashhad Branch, Islamic Azad University, Mashhad, Iran (e-mail: miranian@mshdiau.ac.ir).

P. Rodriguez is with the Department of Electrical Engineering, Technical University of Catalonia, 08222 Terrassa, Spain, and also with Abengoa Research, 41014 Seville, Spain (e-mail: prodriguez@ee.upc.edu).

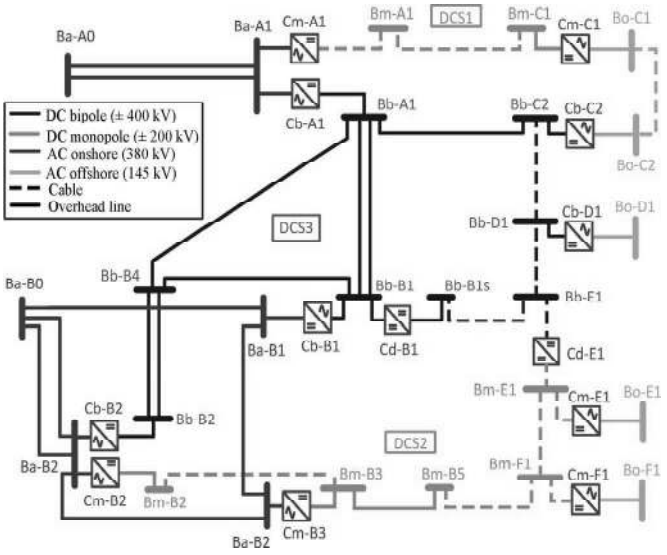

Fig. 1. CIGRE B4 eleven-terminal dc grid with five offshore and six onshore ac buses.

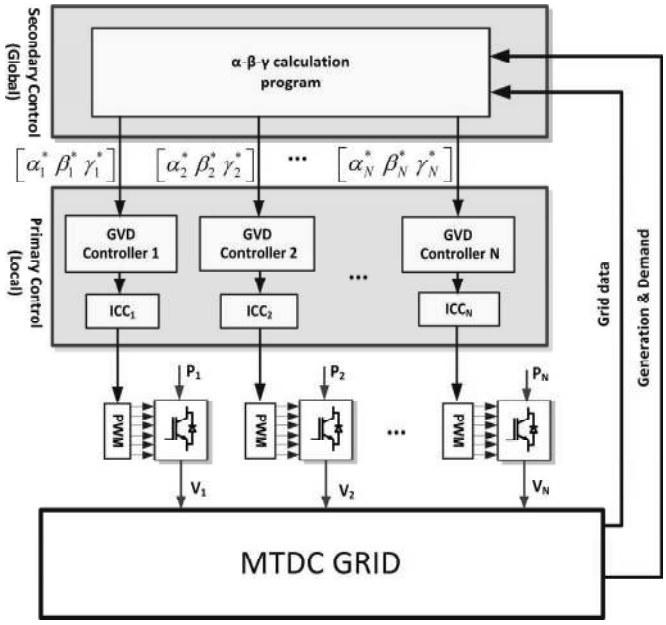

Fig. 2. Proposed hierarchical control framework for the MTDC grids.

give rise to voltage oscillations associated with the voltage margin method [18].

However, despite the popularity of the voltage droop control, it has some drawbacks. The main one lays on the fact that it cannot perform fixed power control for a particular VSC station or fixed dc voltage control, if necessary.

In order to overcome the mentioned shortcoming, in this paper, a generalized voltage droop (GVD) strategy is proposed for performing the voltage control and power control of MTDC grids. The proposed strategy is flexible in terms of power flow and dc voltage control and power sharing based on droop characteristics. In fact, fixed power control and fixed dc voltage control can be both performed using the proposed GVD control strategy with a smooth transition strategy.

The rest of this paper is organized as follows: Section II describes the control structure of the MTDC grids. The GVD is explained in Section III. Simulations of a six-terminal dc test system are presented in Section IV. Finally, the main findings of the paper are summarized in Section V.

II. Control of MTDC Grids

MTDC grids are characterized by the interconnection of several VSC-HVDC systems. Fig. 1 depicts the schematic diagram of the recently released CIGRE B4 MTDC grid [24], interconnecting six ac buses to five offshore grids via 14 dc buses. The main components of the VSC-HVDC terminals include ac circuit breaker, ac transformer, ac filter, phase reactor, VSC, and dc capacitor.

For the effective control of the MTDC grid, a two-layer hierarchical control structure, as illustrated in Fig. 2, is developed in this paper. In this structure, at the upper level (secondary control), the parameters of the voltage droop controllers of the VSCs are determined, according to the grid conditions and demand and generation requirements at the ac sides, and sent to the primary control level.

On the other hand, primary control of MTDC grids includes dc voltage regulation at the dc terminals, control of active and reactive power at the point of common coupling (PCC), and maintaining the PCC's ac voltage at the specified setpoint. The most commonly used control strategy for the VSC-HVDC stations is based on the vector control [18]. In this strategy, the ac currents and voltages of the converter station (at the PCC) are transformed into the rotating direct–quadrature ($d-q$) reference frame, synchronized with the ac grid voltage by means of a phase-locked loop (PLL). This structure permits to carry out a decoupled control of the active and reactive powers as well as the dc and ac voltages. The general architecture of the vector control at a VSC-HVDC station is illustrated in Fig. 3. The outer controllers in Fig. 3 are responsible for generating the reference currents for the inner current controller (ICC), which determines the voltage reference of the converter in the $d-q$ frame.

A. ICC

The ICC, as shown in Fig. 4, includes fast proportional–integral (PI) controllers, which track the reference currents, set by the outer controllers, and produces the voltage reference for the converter. To derive the structure of the ICC, the voltage at PCC (e_s) and the converter-side voltage (v_c) in Fig. 3 are related by

$$e_s - v_c = R_T i_c + L_T \frac{di_c}{dt} \tag{1}$$

where i_c is the current flowing from the ac grid to the converter, and R_T and L_T represent the total resistance and inductance installed between the PCC and the converter. Then, by applying the $d-q$ transformation, (1) can be expressed in the $d-q$ reference frame by

$$c_d - v_d = R_T i_d + L_T \frac{di_d}{dt} - \omega L_T i_q \tag{2}$$

$$e_q - v_q = R_T i_q + L_T \frac{di_q}{dt} + \omega L_T i_d \tag{3}$$

where ω is the angular frequency of the ac voltage at the PCC.

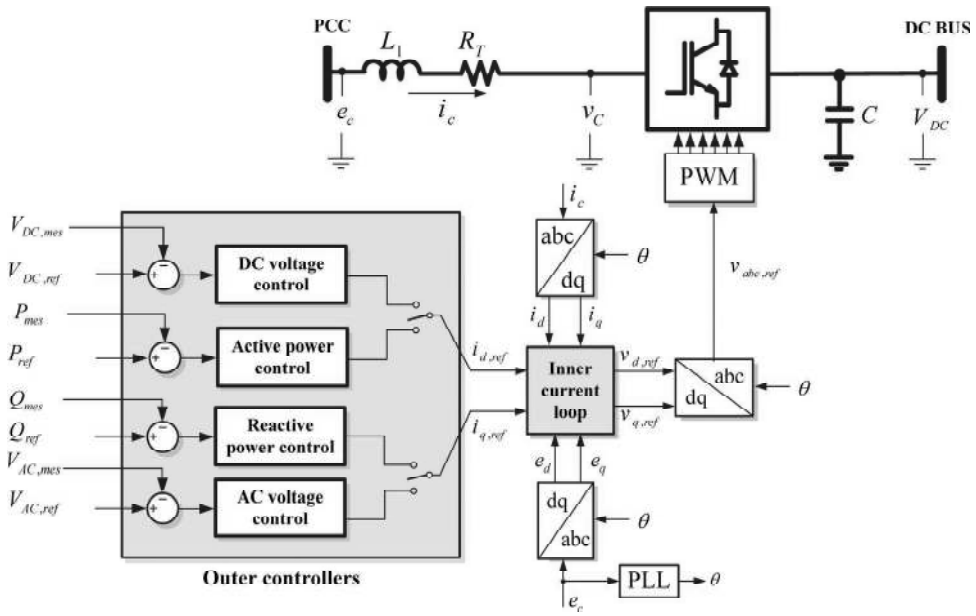

Fig. 3. General architecture of the vector control for a VSC-HVDC station.

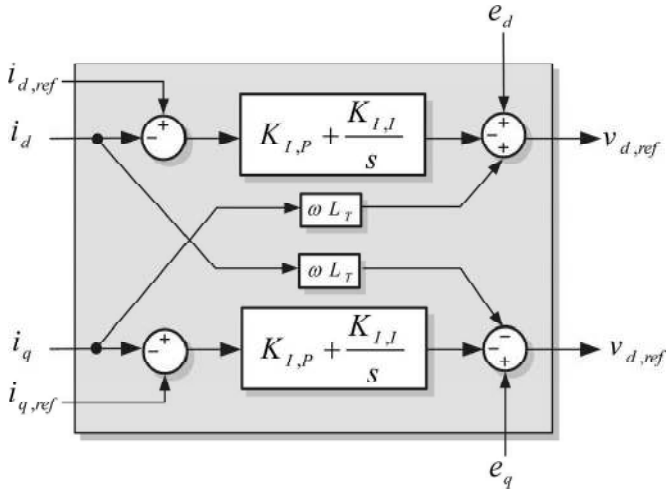

Fig. 4. Structure of the ICC.

The reference voltages ($v_{d,\mathrm{ref}}$ and $v_{q,\mathrm{ref}}$), produced by ICC, are then transformed back into the abc reference frame and used to generate the switching signal of the converter.

B. Outer Controllers

The outer controllers include the active and reactive channels, as shown in Fig. 3. The active channels are responsible for regulating the active power and the dc voltage, while the reactive channels control the reactive power or amplitude of the ac voltage at the PCC.

For active power control, the power equations in the $d-q$ reference frame can be used as

$$P = v_d i_d + v_q i_q \tag{4}$$

$$Q = v_q i_d - v_d i_q. \tag{5}$$

It is worth noting that the d-axis of the $d-q$ frame is aligned with the ac network voltage phasor through a PLL, i.e., $e_q = 0$ and, hence,

$$P = v_d i_d \tag{6}$$

$$Q = -v_d i_q. \tag{7}$$

Based on (6) and (7), the currents in the d- and q-axes can be used to control active and reactive powers, respectively.

The ac voltage controller is intended to regulate the amplitude of the PCC's ac voltage. This can be accomplished by injecting the required amount of reactive power such that the ac voltage at the PCC matches the reference value. Hence, the control of the ac voltage is carried out by modifying the q-axis current.

Likewise, to keep the dc voltage at its reference value, the active power exchanged with the ac grid must be properly regulated. Hence, modification of the d-axis current (i_d) allows to control the dc voltage within the permissible limits.

C. Voltage Droop Control

The voltage level at different terminals of an MTDC grid directly influences the flow of dc power between the terminals of the MTDC grid. It is worth noting that unlike ac transmission systems where fixed and identical voltage amplitudes (normally around 1 p.u.) are preferred throughout the system, the MTDC grids cannot have the same voltage level over the entire system, as the power flow between the dc terminals depend on this variable.

The voltage droop control allows regulating the dc voltage within the grid by adjusting the converter's currents, in such a way that the power balance is guaranteed throughout the grid [19]. In this method, a proportional controller is employed, thus following a characteristic describing a unique relation between the dc voltage and the converter's current [20].

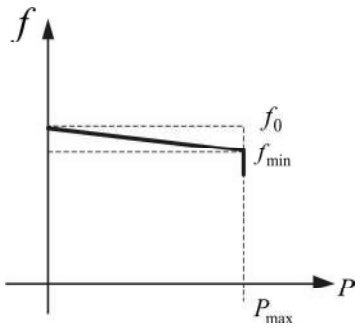

Fig. 5. Power–frequency droop in ac power system.

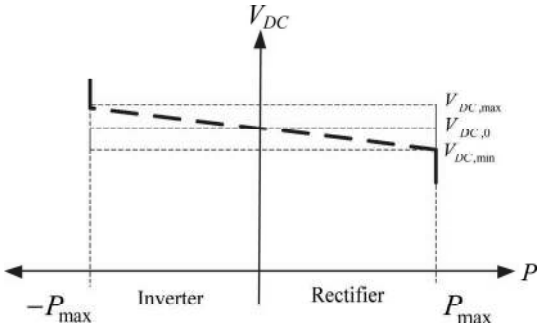

Fig. 6. Conventional (fixed) voltage droop characteristics.

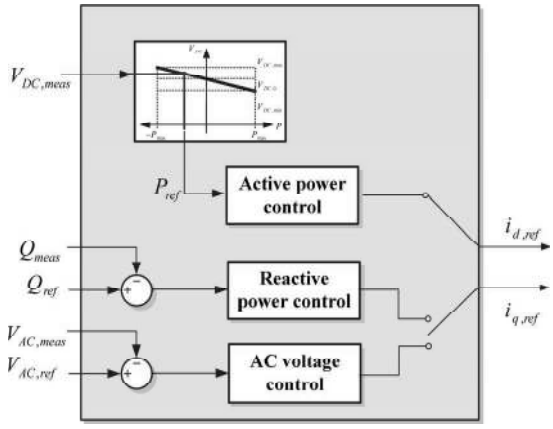

Fig. 7. Implementation of voltage droop control in outer control loop.

The idea behind the voltage droop control has been inspired by the power–frequency droop control in ac networks, where increase/decrease in demand level leads to a frequency drop/rise, as shown in Fig. 5. Similarly, in an MTDC grid, a rise in the dc voltage implies a power surplus in the system, and the dc voltage-regulating stations should start to operate in order to reestablish power balance. Meanwhile, a dc voltage drop indicates lack of power in the system, and the dc voltage-regulating stations should start to increase rectification [21]. This is the basics of the voltage droop control for MTDC grids. A typical voltage droop characteristic shown in Fig. 6 illustrates the idea clearly. In addition, the implementation of voltage droop characteristic inside outer control loop is illustrated in Fig. 7.

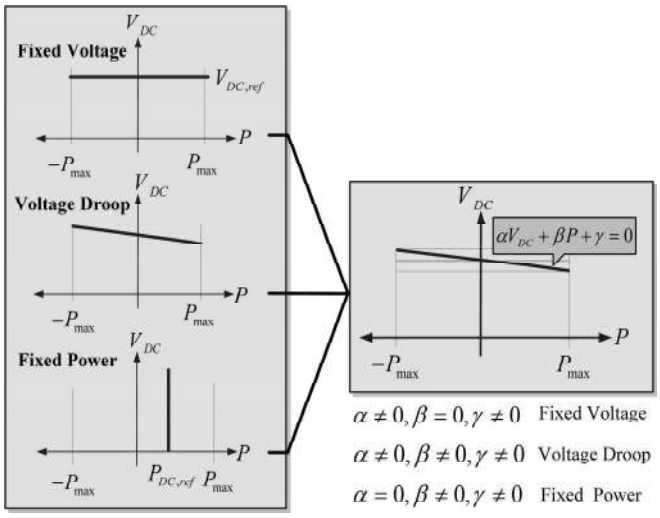

Fig. 8. GVD characteristics with three control modes.

Despite its common applications, the voltage droop control has some drawbacks [22], [23].

- It is not able to perform full power flow control since the droop control cannot fix the active power at a constant level.
- It cannot fix the voltage of the dc terminals, if required.

Hence, modifications should be introduced into the voltage droop control to overcome the aforementioned shortcomings.

III. GVD Control

The GVD is able to perform fixed power control and fixed dc voltage control and to share power among voltage-regulating converters based on the slopes of voltage droop characteristics. It involves three operating modes, as shown in Fig. 8, where each mode can be activated by adjusting the coefficient of the GVD characteristic. The GVD characteristic is mathematically expressed by

$$\alpha V_{\mathrm{DC,meas}} + \beta P_{\mathrm{meas}} + \gamma = 0 \tag{8}$$

where $V_{\mathrm{DC,meas}}$ and P_{meas} are the measured voltage and power at the dc side of the VSC, respectively, and α, β, and γ are the coefficients of the GVD characteristics.

A. Operating Modes of the GVD Control

The operating modes of the GVD control are explained as follows.

1) Mode 1—Conventional Voltage Droop Control: This mode is employed by choosing $\alpha \neq 0$, $\beta \neq 0$, and $\gamma \neq 0$. In this mode, the conventional voltage droop control is carried out, i.e., when converter's dc voltage starts rising, it increases power inversion. On the other hand, if the dc voltage drops, the converter injects more power into the dc grid.

For this operating mode, the GVD coefficients are computed based on the dc voltage ($V_{\mathrm{DC},0}$) and power (P_0) associated

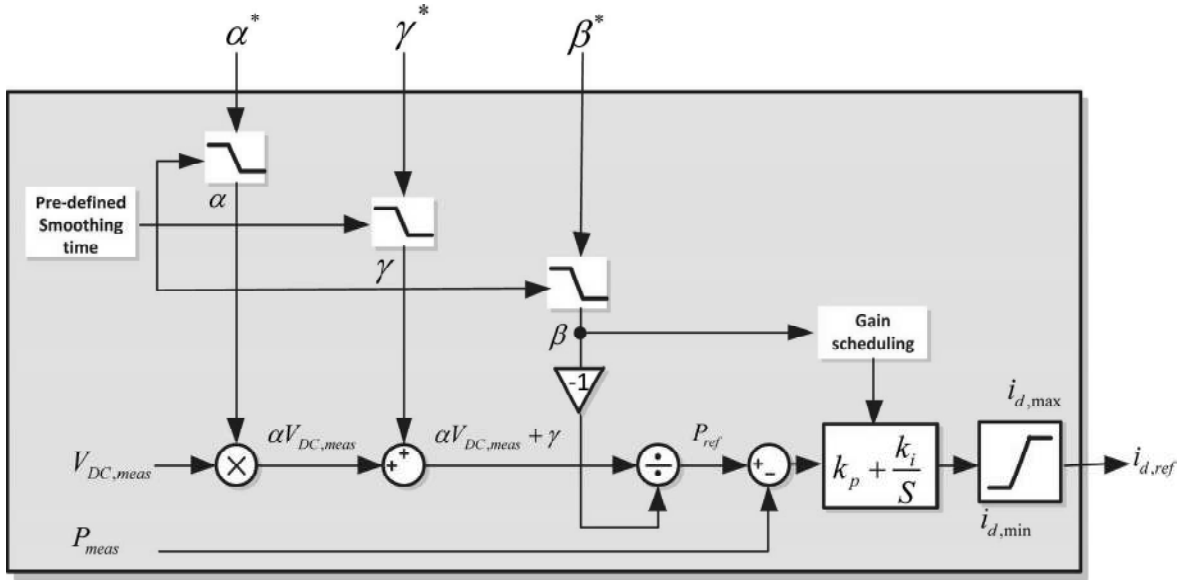

Fig. 9. Implementation of the proposed GVD control with the smooth change in the operating mode.

with an operating point of the corresponding converter. In other words, the following condition must be satisfied:

$$\alpha V_{\mathrm{DC},0} + \beta P_0 + \gamma = 0. \tag{9}$$

In (9), there are three unknown parameters (α, β, and γ). Hence, two more equations must be added to solve for α, β, and γ. In this paper, the slope of GVD characteristics (m) are assumed constant and predefined. Hence,

$$m = \frac{\beta}{\alpha}. \tag{10}$$

Without any loss of generality, by assuming $\alpha = 1$, one can compute

$$\beta = m. \tag{11}$$

Based on (9) and (11), the γ can be determined as

$$\gamma = -V_{\mathrm{DC},0} - mP_0. \tag{12}$$

2) Mode 2—Fixed Power Control: In the second mode of operation, the controller fixes the active power of the station to the specified setpoint, i.e., P_{ref}, by choosing $\alpha = 0$, $\beta \neq 0$, and $\gamma \neq 0$. This mode of operation allows the fixed power control, particularly in circumstances where a station needs to receive or transfer a particular amount of active power while the remaining power is shared among other stations according to their droop characteristics.

In this mode, $\alpha = 0$. Hence, based on (9) and preserving $\beta = m$, which is obtained for the conventional voltage droop mode, i.e.,

$$\alpha = 0 \tag{13}$$
$$\beta = m \tag{14}$$

and by setting $P_0 = P_{\mathrm{ref}}$, γ can be determined as

$$\gamma = -\beta P_{\mathrm{ref}}. \tag{15}$$

According to (15), by adjusting the coefficients β and γ and also setting α to zero, the required reference power is obtained.

3) Mode 3—Fixed DC Voltage Control: The third operating mode controls the dc voltage of the station at the specified setpoint, i.e., $V_{\mathrm{DC,ref}}$, with $\alpha \neq 0$, $\beta = 0$, and $\gamma \neq 0$. This mode of operation is useful when it is required to fix the dc voltage of the station at a particular level. In this control mode, the task of the dc voltage control and the active power balance within the MTDC grid is transferred to the converter station operating in the third mode of the GVD control (such as the slack bus in ac grid).

However, if this mode is activated by directly setting $\beta = 0$, then the reference and measured signals of the active channel must be changed from power to dc voltage via a hard switching element, as shown in Fig. 3. In this paper, a novel strategy is proposed to eliminate this undesirable effect. In this strategy, for constant dc voltage control, the GVD is still operating in the conventional voltage droop mode (i.e., mode 1), but an extremely small value is assigned to coefficient β, which indicates the slope of the GVD characteristics. Hence, the GVD characteristic is almost aligned to the horizontal axis, resembling the fixed voltage control mode. Therefore, in this circumstance, the following reference power signal is generated by the GVD characteristic:

$$P_{\mathrm{ref}} = \frac{\alpha V_{\mathrm{DC,meas}} + \gamma}{-\beta} \tag{16}$$

where $\beta \approx 0$, and according to (12), γ can be written as

$$\gamma = -V_{\mathrm{DC},0} - \beta P_0. \tag{17}$$

Now, assuming that $\alpha = 1$, setting $V_{\mathrm{DC},0} = V_{\mathrm{DC,ref}}$, and substituting (17) into (16) results in Fig. 9, the following error signal is sent to the active channel PI controller:

$$e = P_{\mathrm{ref}} - P_{\mathrm{meas}} = \frac{-1}{\beta}(V_{\mathrm{meas}} - V_{\mathrm{DC,ref}}) + P_0 - P_{\mathrm{meas}}. \tag{18}$$

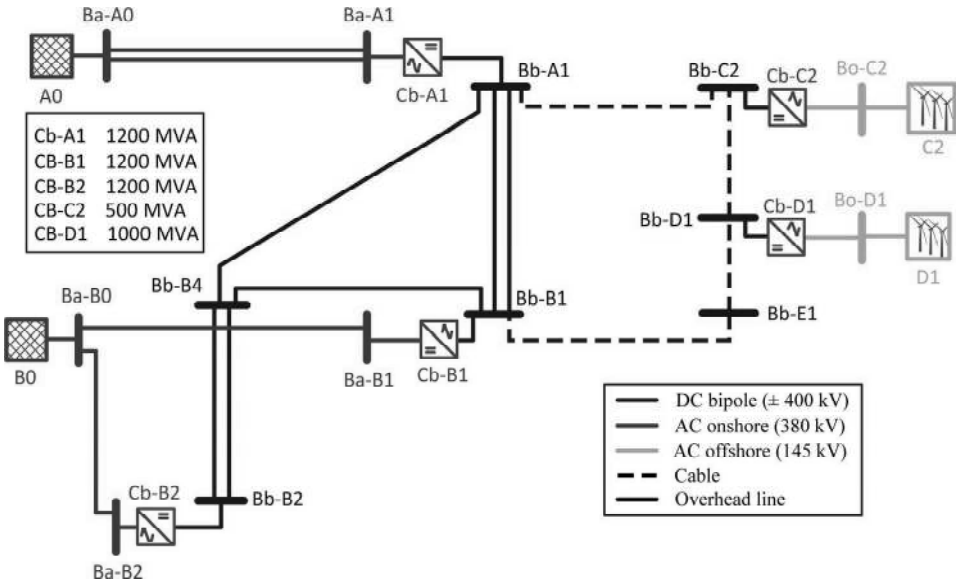

Fig. 10. DCS3 of CIGRE B4 dc grid test system.

Since, voltage and power signals are in per-unit basis (i.e., are in similar range), and the coefficient $1/\beta$ tends to the infinity, the power error term $P_0 - P_{\text{meas}}$ in (18) can be disregarded compared to the voltage error term $V_{\text{meas}} - V_{\text{DC,ref}}$. Hence, (18) can be approximated by

$$c \approx \frac{1}{\beta}(V_{\text{DC,ref}} - V_{\text{meas}}) \tag{19}$$

indicating a fixed dc voltage control action of the GVD control.

It must be noted that the large value of the gain $1/\beta$ in the error signal of (19) may lead to the instability of the control system. To avoid such adverse effect, a gain scheduling block, as illustrated in Fig. 9, decreases the gain of the active channel PI controller smoothly, as β tends to zero.

Therefore, it can be remarked that the proposed GVD strategy has much more flexibility than the conventional voltage droop scheme, which is only capable of power sharing based on the droop characteristics of the VSCs.

B. Smooth Change in GVD Operation Modes

In order to allow a smooth change of the GVD characteristic from one mode to another, a smoothing function is employed. In fact, when the GVD is going to change its operating mode, this is carried out by changing its coefficients, i.e., α, β, and γ are varied from the old values to the new values, smoothly during the smoothing period of $T_{\text{smoothing}}$. This strategy, as illustrated in Fig. 9, improves the transient response of the control system during mode change in the GVD characteristics, as compared with the abrupt change in the GVD coefficients.

Moreover, such a smooth change policy is applied to the coefficients of the active channel PI controller, by gain scheduling of k_p and k_i, as shown in Fig. 9, during transition to the fixed dc voltage control mode.

IV. Simulation and Discussion

The proposed GVD control strategy is evaluated by using the recently released dc grid test system by CIGRE [24]. This test system is developed by CIGRE's B4 working group as a benchmark for conducting dc grid studies and analysis. The CIGRE B4 dc grid test system includes two onshore ac systems; four offshore ac systems; two dc nodes, with no connection to any ac system; and three dc systems. The overall system is comprised of 11 VSC stations.

However, for the sake of clarity in this paper, only the dc system three (DCS3), i.e., a five-terminal bipolar VSC-HVDC meshed grid with a dc-link voltage of ±400 kV, is employed for evaluating the proposed control strategy. The schematic diagram of DCS3 is shown in Fig. 10. It can be seen that two VSCs are connected to offshore ac buses, while other three VSCs serve as the interface between the dc grid and the onshore ac buses (i.e., grid-connected VSCs). The offshore systems are modeled as constant-power sources, and onshore systems are stiff grids represented by ideal voltage sources behind the impedance.

It must be noted that VSCs of the offshore systems adjust the frequency of their corresponding ac system. These VSCs are equipped with a GVD control scheme operated in fixed power mode in parallel with a frequency controller. On the other hand, the VSCs of the onshore systems control the voltage of the dc grid or active power of their corresponding ac system.

A. Grid Data and Modeling

The DCS3 includes five bipolar VSC-HVDC stations with a dc voltage level of ±400 kV. There are two offshore systems with an ac voltage level of 145 kV and six onshore systems with an ac voltage of 380 kV. The dc grid is composed of dc overhead lines (OHLs) and cables, with the specifications presented in Table I. The specifications of the ac OHL are also given in Table I. For each converter station, the total resistance

TABLE I
OHL AND CABLE DATA

Line Data	R [Ω/km]	L [mH/km]	C [μF/km]	G [μS/km]
DC OHL ± 400kV	0.0114	0.9356	0.0123	-
DC cable ± 400kV	0.0095	2.1120	0.1906	0.048
AC OHL 380kV	0.0200	0.8532	0.0135	-

TABLE II
CONVERTER STATION PARAMETERS

VSC station	R_T (Ω)	L_T (mH)	C (μF)
Cb-A1	0.403	33	450
Cb-B1	0.403	33	450
Cb-B2	0.403	33	450
Cb-C2	1.210	98	150
Cb-D1	0.65	49	300

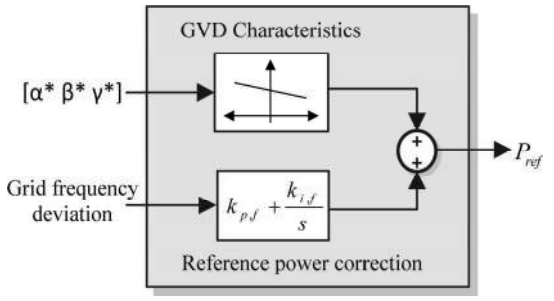

Fig. 11. Implementation of the active channel controller in offshore wind farms with GVD and frequency controller.

and inductance between the VSC and the PCC, i.e., R_T and L_T, respectively, as well as the dc-link capacitor C, have been presented in Table II.

The control mode of VSCs depends on whether they are connected to an offshore or an onshore ac grid. Since the offshore grids are normally weak ac systems, their active channel controls the frequency by a GVD control scheme operated in fixed power mode, working in parallel with a frequency controller, as shown in Fig. 11, while their reactive channel controls the voltage's amplitude of the offshore ac grid. On the other hand, the grid-side converters control the dc voltage of the MTDC grid (or the active power at the PCC) and reactive power at the PCC. It must be noted that the grid-side VSCs employ GVD characteristic at their active channel for the dc voltage control. To maintain power factor at unity, these converters fix the PCC's reactive power at zero. The control functions of the active and reactive channels of the onshore and offshore VSCs are summarized in Table III.

For modeling of the grid, an average-value model of the VSCs has been used. The offshore wind farms have been modeled as constant-power sources. Moreover, the π model has been adopted for the OHLs and the cables.

B. MTDC Grid Startup

Prior to performing the simulation of the different scenarios, the startup condition of the grid will be discussed and simulated.

TABLE III
CONTROL MODES OF VSCS

VSC station	Active channel	Reactive channel
Cb-A1	GVD control	Reactive power control
Cb-B1	GVD control	Reactive power control
Cb-B2	GVD control	Reactive power control
Cb-C2	GVD with Frequency control	AC voltage control
Cb-D1	GVD with Frequency control	AC voltage control

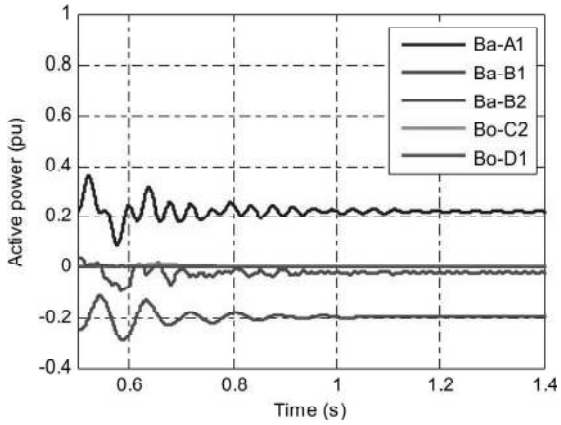

Fig. 12. DC power at converter stations for different voltage intercepts of voltage droop characteristics when there is no offshore generation.

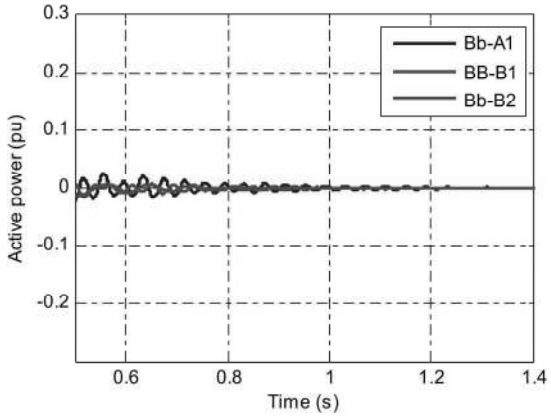

Fig. 13. DC power at converter stations for identical voltage intercepts of voltage droop characteristics when there is no offshore generation.

The startup condition is related to the initial dc voltage of the VSCs when the grids start from a resting state (i.e., no generation by offshore systems). When there is no offshore power generation, it is expected that no power flows within the dc grid. However, in case the different voltage intercepts (i.e., $V_{\mathrm{DC},0}$ in Fig. 6) are not identical, there will be an unexpected flow of power through the grid, even if there is no power injection from the offshore stations. This happens due to the difference between voltage intercepts $(\Delta V_{\mathrm{DC},0})$ of voltage droop characteristics of onshore VSCs. The dc power at the onshore VSCs, considering a situation where there are differences between the voltage intercepts, is shown in Fig. 12. In contrast, Fig. 13 shows the dc power in the case when voltage droop characteristics have identical voltage intercepts.

TABLE IV
BRIEF DESCRIPTION OF SIMULATION SCENARIOS

Scenario no.	Scenario description
1	Power sharing among grid connected converters based on conventional voltage droop.
2	Cb-B1 goes into fixed power control mode, remaining power shared between Cb-A1 and Cb-B2 based on conventional voltage droop.
3	Cb-B1 and Cb-B2 go into fixed power control mode, Cb-A1 goes into fixed DC voltage control mode.

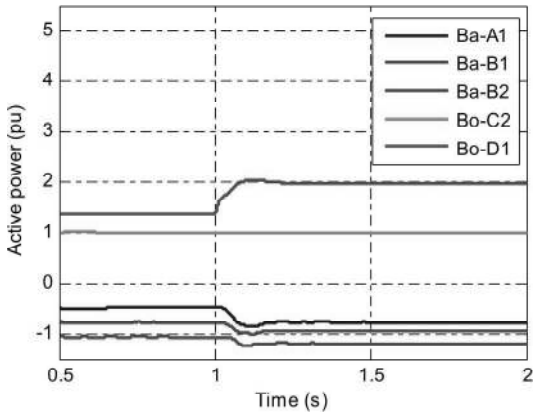

Fig. 14. Active power at converter stations for scenario 1.

To avoid such an undesirable phenomenon in an MTDC grid, the simulations of this paper are initiated with identical voltage intercepts for VSC's GVD characteristics. After the grid startup, the GVD characteristics are adjusted according to the planned power sharing.

C. Simulation Results

In order to investigate the control performance of the proposed approach within an MTDC grid, three simulation scenarios, as presented in Table IV, are implemented.

1) Scenario 1—Conventional Voltage Droop: In the first simulation scenario, the generated power by the offshore systems is shared among grid-side VSCs based on the conventional droop scheme. Figs. 14 and 15 show the active power and dc voltage at all converter stations during this simulation, respectively. The base power and dc voltage for normalization are 500 MVA and 800 kV, respectively.

In this scenario, at $t = 1$ s, the generated power of offshore grid Bo-D1 increases to 2 p.u. This power increase is shared among the grid-side converters based on their droop characteristic.

As stated earlier, the offshore VSCs control the amplitude of the ac voltage at the PCC. The ac voltage amplitude of the offshore grids Bo-C2 and Bo-D1 is shown in Fig. 16. It is shown that, at $t = 1$ s, when the generation by Bo-D1 increases to 2 p.u., there is a transient in the ac voltage amplitude of this offshore grid. The reactive channel of VSC Cb-D1 quickly restores the grid voltage to the reference value of 1 p.u.

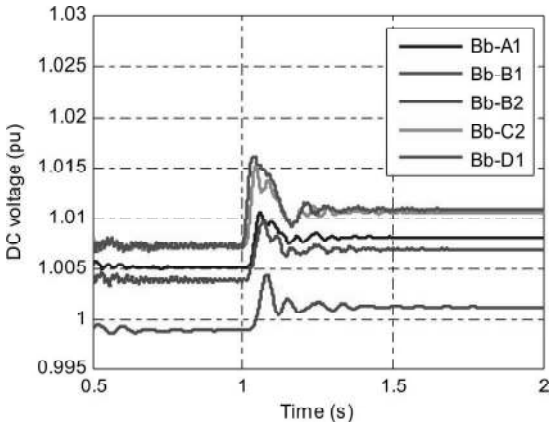

Fig. 15. DC voltage at converter stations for scenario 1.

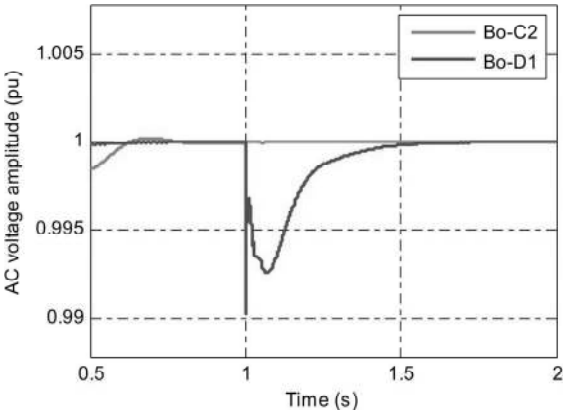

Fig. 16. AC voltage at offshore grids for scenario 1.

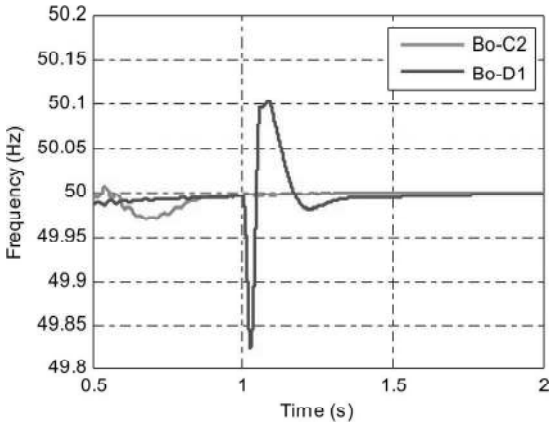

Fig. 17. Frequency at offshore grids for scenario 1.

In addition, the frequency at the offshore grids is depicted in Fig. 17. It is shown that the frequency of the offshore grid Bo-D1 is quickly restored to the reference value of 50 Hz after generation increase at $t = 1$ s. In addition, there is no variation in the frequency of offshore grid Bo-C2, as it is isolated from the other offshore grid.

2) Scenario 2—Fixed Power Control: In the second scenario, the grid condition is similar to the previous scenario prior

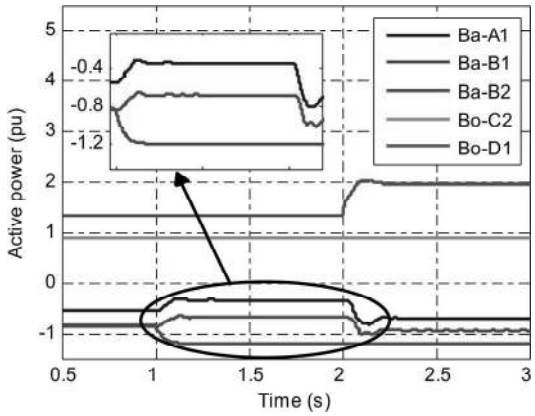

Fig. 18. Active power at converter stations for scenario 2.

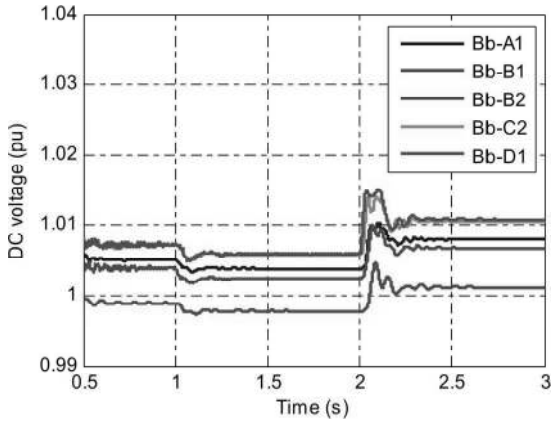

Fig. 19. DC voltage at converter stations for scenario 2.

to $t = 1$. After this time, the onshore grid Ba-B1 demands fixed power of 0.96 p.u. (i.e., its absorbed power must increase from 0.7 p.u. to 1.2 p.u.). This is done by changing the GVD mode of the corresponding VSC from the conventional droop to the fixed power control, which is based on the proposed smooth change strategy. The active power and dc voltage profiles of all VSCs during this simulation are depicted in Figs. 18 and 19, respectively. Moreover, at $t = 2$ s, the generated power by offshore grid Bo-D1 increases to 2 p.u. In this circumstance, the new generation is shared between Ba-A1 and Ba-B2 only since Ba-B1 operates in the fixed power mode. During this development, the variations of the dc voltage of the CB-B1, due to the abrupt GVD characteristic change and smooth change strategy, are compared in Fig. 20, indicating the positive effect of the proposed GVD characteristic smooth change strategy.

The actual and reference d-axis current of VSC Cb-B1 is shown in Fig. 21.

3) Scenario 3—Fixed Voltage Control: In the final simulation scenario, prior to $t = 1$ s, the situation is similar to scenario 1. At $t = 1$ s, both Ba-B1 and Ba-B2 go into fixed power control mode. At $t = 1.5$ s, onshore grid Ba-A1 takes the responsibility of dc grid voltage control and power balance inside the grid by operating the fixed dc voltage mode. The active power and dc voltage profiles during this simulation are depicted in Figs. 22 and 23, respectively. In this scenario, there are two events in the offshore power generation. First, at $t = 2.5$ s, the generation

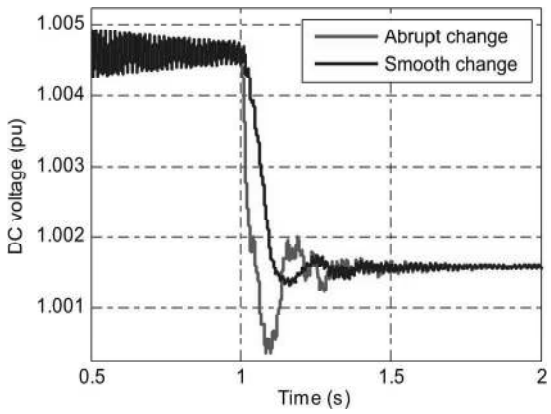

Fig. 20. Variations of the dc voltage of the CB-B1, due to the abrupt GVD characteristic change and smooth change strategy, in scenario 2.

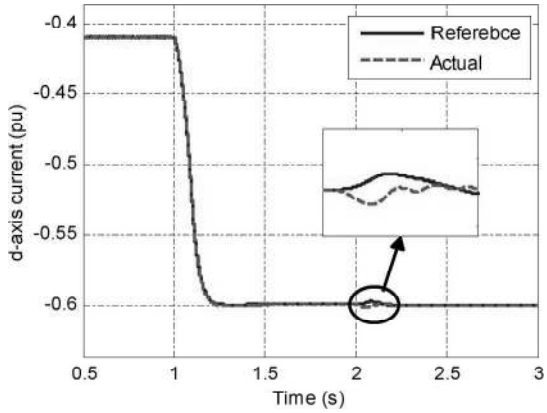

Fig. 21. d-axis current at VSC Cb-B1 for scenario 2.

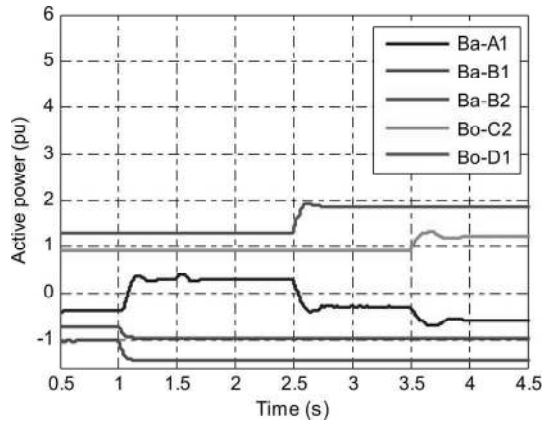

Fig. 22. Active power at converter stations for scenario 3.

by Bo-D1 is increased. This event is followed by an increase in Bo-C2 generation at $t = 3.5$ s. During these events, the dc voltage at VSC Cb-A1 is fixed at 1 p.u., while onshore grid Ba-A1 guarantees the power balance of the dc grid.

The variations of the dc voltage at the CB-A1, which are generated as a result of the abrupt and smooth changes in the GVD characteristic as well as the parameters of the active channel PI controller, are shown in Fig. 24, indicating the considerable performance of the proposed smooth change strategy.

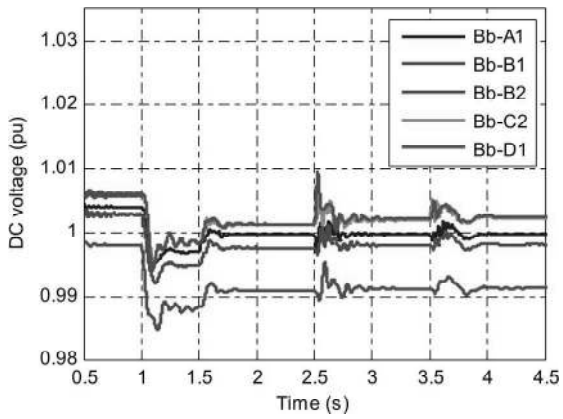

Fig. 23. DC voltage at converter stations for scenario 3.

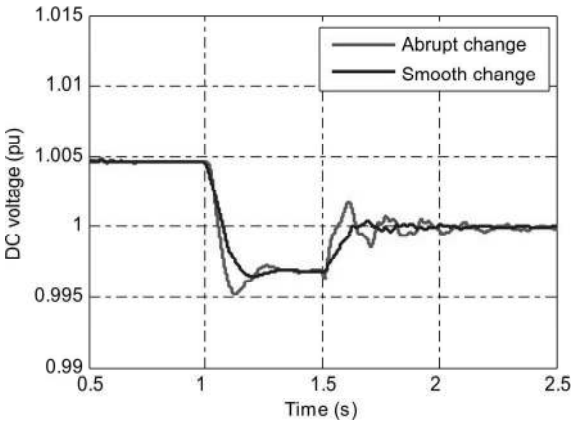

Fig. 24. Variations of the dc voltage of the CB-A1, due to the abrupt GVD characteristic change and smooth change strategy, in scenario 3.

TABLE V
PARAMETERS OF THE ACTIVE CHANNEL PI CONTROLLER

Mode	k_p	k_I
Conventional droop and fixed power	0.5	33
Fixed voltage(Final values)	0.025	1.156

In addition, the values of the proportional and integral gains of the active channel PI controller, in case of conventional voltage droop control and fixed dc voltage control, are presented in Table V.

The amplitude of ac voltages of the offshore grids are shown in Fig. 25, indicating that the voltages at the PCC are maintained at 1 p.u. during variations in offshore generation.

The frequency at offshore grids Bo-C2 and Bo-D1 are shown in Fig. 26. Clearly, the frequency of both grids is quickly restored to the reference value during transients in the generated power.

V. CONCLUSION

This paper has proposed a GVD strategy for voltage control and power sharing in MTDC power systems. The GVD strategy was implemented at the primary level of a two-layer hierarchical control structure. On the other hand, the coefficients of the GVD characteristic were determined at the secondary

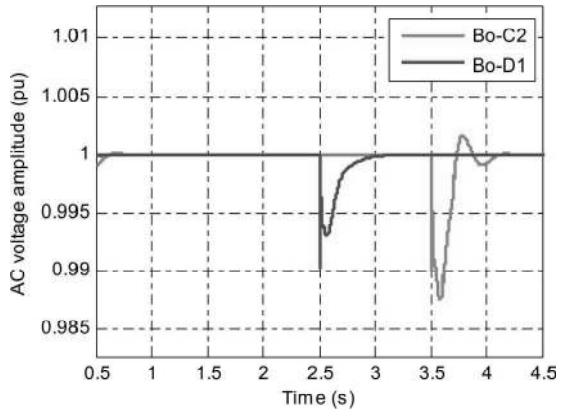

Fig. 25. AC voltage at offshore grids for scenario 3.

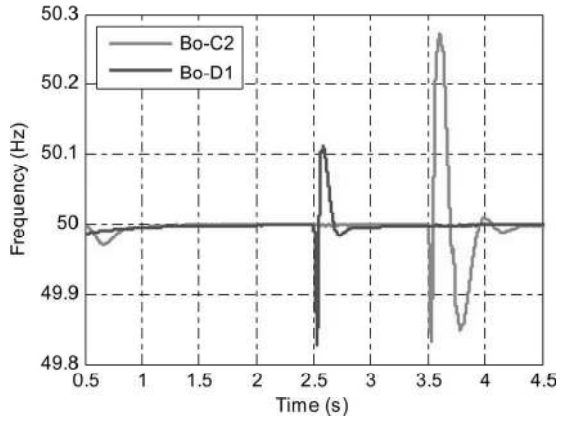

Fig. 26. Frequency at offshore grids for scenario 3.

level of the hierarchical control system. The proposed GVD strategy is able to perform power sharing based on the slope of voltage droop characteristic, fixed active power control, and fixed dc voltage control. Each of the three control modes may be activated by proper adjustment of the coefficients of the proposed GVD characteristics. Moreover, for smooth transition between the control modes of the GVD, a smooth transition strategy has been developed. Simulation results obtained for the DCS3 of CIGRE B4 DC grid benchmark, which is composed of five bipolar VSCs, demonstrated the capabilities and stable operation of the GVD scheme in case of variations in output power of converter stations.

Through the simulations, it has been demonstrated that the proposed control strategy is able to eliminate the control and power-sharing limitations of the conventional voltage droop and enhance the control system maneuverability. In addition, it was shown that switching from one operating mode to another does not result in oscillation in the active powers as a result of implementing a smooth change strategy for adjusting the GVD coefficients.

ACKNOWLEDGMENT

Any opinions, findings, and conclusions or recommendations expressed in this material are those of the authors and do not necessarily reflect those of the host institutions or funders.

REFERENCES

[1] L. Jiao, G. Joos, C. Abbey, Z. Fengquan, and B. T. Ooi, "Multi-terminal DC (MTDC) system for wind farms powered by doubly-fed induction generators (DFIGs)," in *Proc. 35th Annu. IEEE PESC*, Jun. 2004, pp. 1413–1418.

[2] N. R. Chaudhuri, R. Majumder, B. Chaudhuri, J. Pan, and R. Nuqui, "Modeling and stability analysis of MTDC grids for offshore wind farms: A case study on the North Sea benchmark system," in *Proc. IEEE Power Energy Soc. Gen. Meet.*, San Diego, CA, USA, Jul. 2011, pp. 1–7.

[3] L. Livermore, J. Liang, and J. Ekanayake, "MTDC VSC technology and its applications for wind power," in *Proc. 45th Int. UPEC*, Cardiff, U.K., Aug./Sep. 2010, pp. 1–6.

[4] J. Yang, J. E. Fletcher, and J. O'Reilly, "Short-circuit and ground fault analyses and location in VSC-based DC network cables," *IEEE Trans. Ind. Electron.*, vol. 59, no. 10, pp. 3827–3837, Oct. 2012.

[5] L. Tang and B. T. Ooi, "Locating and isolating DC faults in multi-terminal DC systems," *IEEE Trans. Power Del.*, vol. 22, no. 3, pp. 1877–1884, Jul. 2007.

[6] J. Yang, J. E. Fletcher, J. O'Reilly, G. P. Adam, and S. Fan, "Protection scheme design for meshed VSC-HVDC transmission systems of large-scale wind farms," in *Proc. 9th IET Int. Conf. ACDC Power Transmiss.*, Oct. 2010, pp. 1–5.

[7] J. Liang, O. G. Bellmunt, J. Ekanayake, and N. Jenkins, "Control of multi-terminal VSC-HVDC transmission for offshore wind power," in *Proc. 13th EPE Appl.*, Sep. 2009, pp. 1–10.

[8] J. Beerten, D. V. Hertem, and R. Belmans, "VSC MTDC systems with a distributed DC voltage control—A power flow approach," in *Proc. IEEE Trondheim PowerTech*, Jun. 2011, pp. 1–6.

[9] M. Han, L. Xiong, and L. Wan, "Power-synchronization loop for vector current control of VSC-HVDC connected to weak system," in *Proc. IEEE POWERCON*, Oct./Nov. 2012, pp. 1–5.

[10] L. Xu, B. W. Williams, and L. Yao, "Multi-terminal DC transmission systems for connecting large offshore wind farms," in *Proc. IEEE Power Energy Soc. Gen. Meet. Convers. Del. Electr. Energy 21st Century*, Jul. 2008, pp. 1–7.

[11] X. Chen *et al.*, "LCC based MTDC for grid integration of large onshore wind farms in Northwest China," in *Proc. IEEE Power Energy Soc. Gen. Meet.*, Jul. 2011, pp. 1–10.

[12] Y. Fu, Y. Wang, Y. Luo, H. Li, and X. Zhang, "Interconnection of wind farms with grid using a MTDC network," in *Proc. 38th Annu. IEEE IECON*, Oct. 2012, pp. 1031–1036.

[13] X. Chen, "Integrating wind farm to the grid using hybrid multiterminal HVDC technology," *IEEE Trans. Ind. Appl.*, vol. 47, no. 2, pp. 965–972, Mar./Apr. 2011.

[14] J. Blau, "Europe plans a North Sea grid," *IEEE Spectr.*, vol. 47, no. 3, pp. 12–13, Mar. 2010.

[15] L. Xu and L. Yao, "DC voltage control and power dispatch of a multi-terminal HVDC system for integrating large offshore wind farms," *IET Renew. Power Generation*, vol. 5, no. 3, pp. 223–233, May 2011.

[16] P. Rault, F. Colas, X. Guillaud, and S. Nguefeu, "Method for small signal stability analysis of VSC-MTDC grids," in *Proc. IEEE Power Energy Soc. Gen. Meet.*, San Diego, CA, USA, Jul. 2012, pp. 1–7.

[17] N. R. Chaudhuri and B. Chaudhuri, "Adaptive droop control for effective power sharing in multi-terminal DC (MTDC) grids," *IEEE Trans. Power Syst.*, vol. 28, no. 1, pp. 21–29, Feb. 2013.

[18] R. T. Pinto, S. F. Rodrigues, P. Bauer, and J. Pierik, "Comparison of direct voltage control methods of multi-terminal DC (MTDC) networks through modular dynamic models," in *Proc. 14th EPE Appl.*, Aug./Sep. 2011, pp. 1–10.

[19] T. M. Haileselassie and K. Uhlen, "Impact of DC line voltage drops on power flow of MTDC using droop control," *IEEE Trans. Power Syst.*, vol. 27, no. 3, pp. 1441–1449, Aug. 2012.

[20] F. D. Bianchi and O. Gomis-Bellmunt, "Droop control design for multi-terminal VSC-HVDC grids based on LMI optimization," in *Proc. 50th IEEE CDC-ECC*, Dec. 2011, pp. 4823–4828.

[21] K. Rouzbehi, A. Miranian, A. Luna, and P. Rodriquez, "Optimized control of multi-terminal DC grids using particle swarm optimization," in *Proc. EPE Appl.*, Lille, France, Sep. 3–6, 2013, pp. 1–9.

[22] K. Rouzbehi, A. Miranian, A. Luna, and P. Rodriquez, "A novel approach for voltage control of multi-terminal DC grids with offshore wind farms," in *Proc. IEEE ECCE Asia Downunder*, Melbourne, Australia, Jun. 2013, pp. 965–970.

[23] K. Rouzbehi, A. Miranian, A. Luna, and P. Rodriquez, "A generalized voltage droop strategy for control of multi-terminal DC grids," in *Proc. 5th ECCE*, Denver, CO, USA, Sep. 15–19, 2013, pp. 59–64.

[24] CIGRE B4 Working Group, (visited 19 Sep. 2013). [Online]. Available: http://b4.cigre.org/Publications/Documents-related-to-the-development-of-HVDC-Grids

Kumars Rouzbehi (S'11) received the B.Sc. and M.Sc. degrees in electrical engineering (with first-class honors) from Islamic Azad University of Iran (IAU), Tehran, Iran, in 1998 and 2001, respectively. Since 2011, he has been working toward the Ph.D. degree at the Technical University of Catalonia (UPC), Terrassa, Spain.

In 2004, he joined the Department of Electrical Engineering, Islamic Azad University (IAU), Mashhad, Iran, where he was selected as a Distinguished Lecturer several times. In parallel with teaching and research at IAU, he was a Director Manager with Khorasan Electric and Electronics Industries Researches (KHEEIR) company until 2011. He has coauthored one book and has been involved in several industrial projects and educational programs in the fields of power systems and power electronics. His research interests include computational intelligence and its applications in the field of power systems, integration of distributed generation systems to the grid, high-voltage dc technology, and particularly control and operation of multiterminal dc grids.

Mr. Rouzbehi has been a member of Amvaje-e-bartar (an Iranian journal of electrical engineering) and policy-making committees and the Editor of *Power System Division*, since 2006.

Arash Miranian (S'11) was born in Mashhad, Iran, in 1983. He received the B.Sc. degree in electrical engineering from Ferdowsi University of Mashhad, Mashhad, Iran, in 2006.

From 2010 to 2011, he was working as a Design Engineer on transmission substation design and construction projects. At the end of 2011, he joined the Institute for International Energy Studies, Tehran, Iran, as a Senior Researcher and focused on modeling and prediction of energy (particularly oil and gas) price and demand and published several papers based on the findings of his research. He has also been involved in several research projects, centering on developing computational intelligence (CI)-based approaches for modeling, identification, prediction, and control. As another research orientation, he is also conducting research on simulation and control in multiterminal dc (MTDC) power systems. Currently, he is with the Young Researchers and Elite Club, Mashhad Branch, Islamic Azad University, Mashhad, Iran. His main research interests lie in CI and its applications in the area of nonlinear system identification and control, with a focus on electric power systems, signal processing and time-series prediction, and simulation and control of (MTDC) power systems.

Jose Ignacio Candela (S'99–M'04) received the B.S., M.S., and Ph.D. degrees from the Technical University of Catalonia (UPC), Terrassa, Spain, in 1987, 2000, and 2009, respectively, all in industrial engineering.

He became an Assistant Professor in 1991 and has been an Associate Professor since 1993 with UPC. He has authored or coauthored more than 30 published technical papers and has been involved in several industrial projects and educational programs in the fields of power quality conditioning and motor drives. His current research interests include power conditioning, integration of distributed energy systems, and control of power converters and motor drives.

Alvaro Luna (S'07–M'10) received the B.Sc., M.Sc., and Ph.D. degrees from the Technical University of Catalonia (UPC), Terrassa, Spain, in 2001, 2005, and 2009, respectively, all in electrical engineering.

In 2005, he joined as a Faculty Member the UPC, where he is currently an Assistant Professor. His research interests include wind turbine control, integration of distributed generation, and power conditioning.

Pedro Rodriguez (S'99–M'04–SM'10–F'14) received the M.Sc. and Ph.D. degrees in electrical engineering from the Technical University of Catalonia (UPC), Terrassa, Spain, in 1994 and 2004, respectively.

He was a Postdoctoral Researcher with the Center for Power Electronics Systems (CPES), Virginia Polytechnic Institute and State University, Blacksburg, VA, USA, in 2005 and with the Department of Energy Technology, Aalborg University (AAU), Aalborg East, Denmark, in 2006. In 1990, he joined as an Assistant Professor the faculty of UPC, where he became the Director of the Research Center on Renewable Electrical Energy Systems (SEER) in the Department of Electrical Engineering. From 2007 to 2011, he was also a Visiting Professor at the AAU, acting as a cosupervisor of the Vestas Power Program. He still lectures Ph.D. courses at the AAU every year. Since 2011, he has been the Head of Electrical Engineering Division at Abengoa Research, Seville, Spain, although he is still with the UPC as a Part-Time Professor. He has coauthored one book and more than 200 papers published in technical journals and conference proceedings. He is the holder of seven licensed patents. His research interests include integration of distributed generation systems, smart grids, and design and control of power converters.

Dr. Rodriguez serves as a member of the Administrate Committee of the IEEE Industrial Electronics Society (IES), as the General Chair of IEEE-IES Gold and Student Activities, as the Vice-Chair of the Sustainability and Renewable Energy Committee of the IEEE Industry Applications Society, and as a member of the IEEE-IES Technical Committee on Renewable Energy Systems. He is a member of the Horizon 2020 Advisory Group on Energy. He is an Associate Editor of the IEEE TRANSACTION ON POWER ELECTRONICS. He was a recipient of the Best Technical Letter Award 2012 and the Second Best Paper Award 2012 from the IEEE TRANSACTIONS ON POWER ELECTRONICS.